Published in final edited form as:

Neuron. 2017 June 21; 94(6): 1132–1141.e4. doi:10.1016/j.neuron.2017.06.009.

Molecular mechanism of MDGA1: regulation of neuroligin 2:neurexin trans-synaptic bridges

Shanti Pal Gangwar[1,2], **Xiaoying Zhong**[1,2], **Suchithra Seshadrinathan**[1,2], **Hui Chen**[3], **Mischa Machius**[1,2], and **Gabby Rudenko**[1,2,#]

[1]Dept. of Pharmacology and Toxicology, University of Texas Medical Branch, Galveston TX, 77555, USA

[2]Sealy Center for Structural Biology and Molecular Biophysics, University of Texas Medical Branch, Galveston TX, 77555, USA

[3]University of Michigan, Ann Arbor, MI, 48109, USA

Summary

Neuroligins and neurexins promote synapse development and validation by forming trans-synaptic bridges spanning the synaptic cleft. Select pairs promote excitatory and inhibitory synapses, respectively, with neuroligin 2 (NLGN2) limited to inhibitory synapses and neuroligin 1 (NLGN1) dominating at excitatory synapses. The cell surface molecules, MAM domain-containing glycosylphosphatidylinositol anchor 1 (MDGA1) and 2 (MDGA2), regulate trans-synaptic adhesion between neurexins and neuroligins, impacting NLGN2 and NLGN1, respectively. We have determined the molecular mechanism of MDGA action. MDGA1 Ig1–Ig2 is sufficient to bind NLGN2 with nanomolar affinity; its crystal structure reveals an unusual locked rod-shaped array. In the crystal structure of the complex, two MDGA1 Ig1–Ig2 molecules each span the entire NLGN2 dimer. Site-directed mutagenesis confirms the observed interaction interface. Strikingly, Ig1 from MDGA1 binds to the same region on NLGN2 as neurexins do. Thus, MDGAs regulate the formation of neuroligin-neurexin trans-synaptic bridges by sterically blocking access of neurexins to neuroligins.

Keywords

MDGA; neurexin; neuroligin; synaptic organizer; adhesion molecule

[#]To whom correspondence should be addressed: G. Rudenko, University of Texas Medical Branch, 301 University Blvd. Galveston, TX 77555, USA, Tel.: (409) 772-6292, garudenk@utmb.edu.

Author Contributions

G.R. and S.P.G. conceived the project. X.Z, S.S., H.C. and S.P.G. performed molecular biology, protein purification and/or crystallization. S.P.G. carried out the binding studies, data collection and analysis of the structures. G.R. and M.M. carried out the structure determinations. G.R. and S.P.G. wrote the paper.

Introduction

Synaptic adhesion and organizing molecules, also known as ‘synaptic organizers’, play an essential role in the development of synapses, the contact and communication points between neurons. The synaptic organizers, neuroligins and neurexins, extend their extracellular domains out into the synaptic cleft where they form trans-synaptic bridges with each other (reviewed Reissner et al., 2013). Interaction of neuroligins with neurexins promotes the development of synapses and normal synaptic transmission (Reissner et al., 2013). Recently, it was discovered that a third family of cell surface molecules, the MDGAs (MAM domain-containing glycosylphosphatidylinositol anchors), regulates the trans-synaptic interaction between neuroligins and neurexins (Connor et al., 2016; Lee et al., 2013; Pettem et al., 2013), though the underlying molecular mechanism is unknown.

Neuroligins and neurexins form large families of adhesion molecules and their members are implicated in neuropsychiatric disease. In humans, five neuroligin genes (*NLGN1*, *NLGN2*, *NLGN3*, *NLGN4X* and *NLGN4Y*) and three neurexin genes (*NRNX1, NRXN2*, and *NRXN3*) exist (Bemben et al., 2015; Reissner et al., 2013). Both neuroligins and neurexins are diversified through alternative splicing of mRNA transcripts; in particular, NLGN2 can accommodate a splice insert at site A, while NLGN1 can carry a splice insert at site A as well as a second splice insert at site B (Boucard et al., 2005; Chih et al., 2006; Schreiner et al., 2014; Schreiner et al., 2015; Treutlein et al., 2014). Neuroligin 2 (NLGN2) localizes specifically to inhibitory synapses, while neuroligin 1 (NLGN1 +site B) is predominant at excitatory synapses (Chubykin et al., 2007; Futai et al., 2013; Gibson et al., 2009; Levinson et al., 2005; Varoqueaux et al., 2004). Splice inserts can regulate the affinities of neuroligins and neurexins for their protein partners (reviewed Reissner et al. 2013). Strikingly, lesions in both neurexins and neuroligins are implicated in autism spectrum disorder and schizophrenia (Bena et al., 2013; Bougeron, 2016; Reissner et al., 2013; Sun et al., 2011). Because these molecules impact the development of excitatory synapses and inhibitory synapses differentially, malfunction of select neuroligin and neurexin members is thought to lead to an imbalance in excitation versus inhibition disrupting neural circuits critical to cognition and behavior (Lee et al., 2016).

MDGAs (MDGA1 and MDGA2) regulate the interaction between neuroligins and neurexins. MDGAs are also implicated in autism spectrum disorder and schizophrenia (Bucan et al., 2009; Kähler et al., 2008; Li et al., 2011). During neural development, MDGA1 controls the radial migration of cortical neurons (Ishikawa et al., 2011; Takeuchi & O’Leary, 2006), but it continues to be expressed postnatally at high levels as well (Lee et al., 2013). MDGAs are composed of six immunoglobulin (Ig) domains, a fibronectin type III (FNIII) domain and a MAM (meprin, A5 protein, PTPμ) domain, and they are tethered putatively to the post-synaptic membrane by a glycosylphosphatidylinositol (GPI) anchor (Litwack et al., 2004). MDGA1 binds specifically to NLGN2 with nanomolar affinity, but not to NLGN1 or NLGN3, forming a side-by-side (*in-cis*) complex involving the extracellular domains; by contrast, MDGA2 prefers to interact with NLGN1 (Connor et al., 2016; Lee et al., 2013; Pettem et al., 2013). The interaction of MDGA1 with NLGN2 blocks the ability of NLGN2 to form a trans-synaptic bridge with neurexins, thus downregulating the ability of NLGN2 to promote inhibitory synapse development; on the other hand, there is

consensus that MDGA2 downregulates excitatory synapse formation (Connor et al., 2016; Lee et al., 2013; Loh et al., 2016; Pettem et al., 2013).

The three-dimensional structure of MDGA1 and the molecular mechanism by which it binds NLGN2 are unknown. Previous studies have revealed that the first three Ig domains of MDGA1 are sufficient to bind NLGN2 (Lee et al., 2013; Pettem et al. 2013). But it is not clear how MDGA1 regulates the interaction of NLGN2 with neurexins. NLGN2 forms an ellipsoidal dimer in the synaptic cleft; each monomer is composed of a globular cholinesterase domain and a helical dimerization domain that contributes two helices to the dimerization interface (Koehnke et al., 2008). A post-synaptically tethered neuroligin dimer forms a neurexin:neuroligin trans-synaptic bridge by recruiting to each of its lateral sides a pre-synaptically tethered neurexin via a select LNS domain (Arac et al., 2007; Chen et al., 2008; Fabrichny et al., 2007; Leone et al., 2010). To understand how MDGA1 regulates the NLGN2:neurexin trans-synaptic bridge, we embarked on molecular and structural studies of these proteins. We show that MDGA1 Ig1–Ig2 is sufficient to bind NLGN2 with nanomolar affinity, and determine the crystal structures of MDGA1 Ig1–Ig2 (2.7 Å) and the complex between NLGN2 and MDGA1 Ig1–Ig2 (4.1 Å). We elucidate the molecular mechanism by which the synaptic organizer MDGA1 can downregulate inhibitory synapse development and reveal the first structure of the NLGN2 ectodomain in complex with a protein partner.

Results

We over-expressed the extracellular domains of MDGA1 and NLGN2 (Fig. 1a) and obtained pure, monodisperse preparations (Fig. 1b and 1c; Fig. S1). We also generated a panel of MDGA1 fragments in order to map the minimal domains required to bind NLGN2 (Fig. 1d). To measure interaction between MDGA1 and NLGN2 in solution, we designed a fluorescence polarization-based (FP) assay and revealed that full-length ectodomains of MDGA1 and NLGN2 bind each other with a K_D of 48 ± 13 nM (Fig. 1e and 1f). MDGA1 Ig1–Ig3 bound NLGN2, in agreement with Pettem et al., 2013 and Lee et al., 2013, however the shorter Ig1–Ig2 construct was sufficient to bind NLGN2 with a K_D of 21 ± 16 nM (Fig. 1e and 1f). Ig2–Ig3 did not bind NLGN2 significantly, nor the isolated domains, Ig1 and Ig3; unfortunately, we could not test Ig2 because we were unable to over-express it. Taken together, our data suggest that the MDGA1 Ig1–Ig2 array is sufficient and required to bind NLGN2.

To gain insight into the architecture of the MDGA1 Ig1–Ig2 tandem, we determined its crystal structure to a resolution of 2.7 Å (Fig. 2a, 2b and Table 1). Ig1 adopts an eight-stranded β-sandwich composed of a three-stranded β-sheet (β1, β4 and β6) and a five-stranded β-sheet (β2, β3, β5, β7 and β8). With the exception of strands β2, β3 and loop β5–β6, the core of Ig1 is reminiscent of domains found in perlecan, the FGF receptor 2 and synCAM. Ig2 adopts a classical C-type seven-stranded immunoglobulin fold composed of a three-stranded β-sheet (β11, β14 and β15) and a four-stranded β-sheet (β9, β10, β12 and β13), like domains found in DSCAM1 and NCAM2. The MDGA1 Ig1–Ig2 tandem forms a rigid, rod-shaped molecule, stabilized by two intradomain and one interdomain disulfide bonds. In both Ig1 and Ig2, the middle strand in the three-stranded β-sheet is disulfide-bonded to an inner strand of the opposing β-sheet, i.e. Cys^{60} and Cys^{108} link strand β4 and

strand β7 together in Ig1, while Cys^{157} and Cys^{214} link strand β10 and strand β14 in Ig2. This feature is known to contribute to the structural stability of Ig-like domains (Hagihara and Saerens, 2014). Several striking, structural features stabilize the interface between Ig1 and Ig2 (Fig. 2c). Strand β8 crosses from Ig1 into Ig2. On one side of strand β8, a large hydrophobic residue (Tyr^{128}) packs underneath a tripartite ionic interaction (Glu^{52}, Arg^{100}, Asp^{130}) that connects loop β3–β4, loop β6–β7, and loop β8–β9. On the other side of strand β8, a disulfide bond between Cys^{36} (Ig 1) and Cys^{222} (Ig2) covalently locks the domains together. Additional residues further stabilize the interface between Ig1 and Ig2 (in particular Val^{37}, Thr^{49}, Ile^{50}, Arg^{51}, Asp^{125}, Val^{126}, Gln^{127}, Asn^{162}, Pro^{163}, Val^{221}, Gly^{223}, Ile^{224} and Pro^{225}). The intersubunit disulfide bond between two tandem Ig domains is unusual. Inspection of more than 1200 structures with two or more consecutive Ig domains, revealed only two other structures where a disulfide bond locks two sequential Ig domains together (siglec-5 (PDB ID:2zg1) and the light chain of an IgG specific for amyloid prefibrillar oligomers (PDB ID:4hbc)). Analysis of the interactions between MDGA1 Ig1 and Ig2, the significant surface they bury (~715 $Å^2$), and conservation of this interdomain disulfide bond in the MDGA family (Fig. S2), further support that these two domains are locked in place with respect to each other.

To understand how MDGA1 interacts with NLGN2, we determined the crystal structure of MDGA1 Ig1–Ig2 in complex with NLGN2 to a resolution of 4.1 Å (Table 1). The crystals exhibit the symmetry of space group P1 and contain three complexes in the asymmetric unit (~4300 residues in total). Each complex consists of an NLGN2 dimer with two MDGA1 Ig1–Ig2 tandems bound. The molecular packing permitted us to exploit six-fold non-crystallographic symmetry restraints, enabling stable refinement of the atomic model despite the relatively low resolution of the diffraction data and the massive protein content (580 kDa; 33,540 atoms). The structure of the complex reveals that MDGA1 Ig1 and Ig2 both bind NLGN2 and that the tandem straddles the NLGN2 dimer with each Ig domain interacting with a different NLGN2 monomer (Fig. 3a and 3b). Molecular interactions underlying the binding mechanism are shown in Fig. 3c and 3d, see also Fig. S3. MDGA1 Ig1 docks on NLGN2 using strands β3, β5, β7, and β8; in turn NLGN2 binds MDGA1 Ig1 via the long loop α10–α11, helix α11 and several residues from loop α4–α5 and loop α6–α7. In total, 16 residues of MDGA1 Ig1 and 21 residues of NLGN2 form interactions closer than 5 Å. Prominent residues from Ig1 include Ile^{119}, Tyr^{107}, and Ser^{121} docking onto NLGN2. Intermolecular ionic interactions link the two proteins together, involving residues from MDGA1 (Arg^{105}, Lys^{109}, Arg^{123}) and residues from NLGN2 (Glu^{281}, Asp^{362}, Glu^{372}). MDGA1 Ig2 binds NLGN2 using strands β9, β10, β12, and β13 which form the concave side of the β-sandwich and embrace two helices from NLGN2, α13 (a helix from the helix-loop-helix EF hand) and α14 (part of the dimerization domain). In total, 17 residues of MDGA1 Ig2 and 18 residues of NLGN2 form interactions closer than 5 Å. A large hydrophobic cluster comprised of residues from Ig2 (Val^{198}, Lys^{200}, Phe^{154}, Tyr^{187}, His^{137}, Arg^{156}, Pro^{189}) forms a hydrophobic surface that packs against two prominent residues from NLGN2, Phe^{408} and Arg^{428}. The NLGN2 residue Arg^{428} is part of a network of ionic interactions on the surface of NLGN2, which also includes Asp^{407}, Asp^{425}, Glu^{429} and Lys^{432}. The interface is also stabilized by a charge cluster formed by three residues from Ig2 (Lys^{202}, Asp^{185}, and Lys^{200}) and two residues from NLGN2 (Asp^{415} and Lys^{424}) as well as

a smaller hydrophobic cluster at the edge of the interface involving Ig2 (Tyr^{191} and Leu^{190}) and NLGN2 (Trp^{438} and Arg^{447}). The interdomain disulfide bond Cys^{36}–Cys^{222} helps stabilize the conformation of the two Ig domains with respect to each other, as the tandem docks onto the NLGN2 dimer.

To validate the interaction between MDGA1 and NLGN2 observed in the crystal structure, we replaced key residues found at the interface with alanine residues or oppositely charged residues and tested their binding (Fig. 3e, 3f, and 3g). Mutations at the interface between Ig1 and NLGN2 (NL2–Mut1, NL2–Mut4 and MDGA1 C8_Mut2 and MDGA1 C8_Mut5) severely disrupted binding between the MDGA1 Ig1–Ig2 tandem and NLGN2 in solution, e.g., mutations on the NLGN2 surface decreased the binding affinity ~10x or more. Likewise, mutations at the interface between Ig2 and NLGN2 (MDGA1 C8_Mut3) disrupted binding of the complex, as did more dramatic combinations of mutations that targeted both Ig1 and Ig2 binding to NLGN2 (NL2–Mut3, NL2–Mut5, MDGA1 C8_Mut1 and MDGA1 C8_Mut4). We also tested NL2–Mut6 (Leu^{374}Ala, Asn^{375}Ala, Asp^{377}Ala); this variant is similar to a previously described mutant, NL2–32 (Glu^{281}Ala, Leu^{374}Ala, Asn^{375}Ala, Asp^{377}Asn) which, in cell-based assays, prevented binding to MDGA1 as well as binding to neurexins (Lee et al., 2013), though the molecular basis for its effect on MDGA1 binding was not known. NL2–Mut6 also replaces the equivalent residues as the NLGN1 mutant NL1–5 (Leu^{399}Ala/Asn^{400}Ala/Asp^{402}Asn) which, when expressed on the cell surface, bound the soluble Ig-fusion protein of neurexin 1β, though it had reduced affinity in surface plasmon resonance experiments (K_D >10 μM) (Arac et al., 2007; Ko et al., 2009). The mutant NL2-Mut6 bound MDGA1 Ig1–Ig2 poorly, and indeed, residues Leu^{374}, Asn^{375}, and Asp^{377} locate to the binding site for MDGA1 Ig1. To confirm that decreased complex formation was not the result of improperly folded proteins, we also tested binding of the NLGN2 mutants to a fragment of neurexin 1α, n1α L5L6 (which contains the C-terminal domains L5, EGF-C and L6), and showed that they all bound neurexin about as well as wild type NLGN2 (Fig. 3f). Together, the mutational analysis confirms that the interface observed between MDGA1 Ig1–Ig2 and NLGN2 in the crystal structure is physiologically relevant.

To understand how MDGA1 can interfere with the binding of neurexins to NLGN2, we mapped the region of neuroligin that binds neurexin (known from crystal structures of NLGN1 and NLGN4 in complex with neurexin 1β; e.g., Arac et al., 2007; Chen et al., 2008; Fabrichny et al., 2007; as well as mutagenesis studies, *e.g.*, Ko et al. 2009) onto NLGN2 in the complex with MDGA1 Ig1–Ig2. We also confirmed that neurexin can compete with MDGA1 for NLGN2 binding with purified proteins (Fig. S4). It is clear that Ig1 of MDGA1 shares a binding site on NLGN2 that partially overlaps the region where neurexins bind neuroligins (Fig. 4a). We conclude that MDGA1 can regulate the formation of trans-synaptic bridges between NLGN2 and neurexins by sterically occluding the neurexin binding site (Fig. 4b).

A striking selectivity has been observed between MDGAs and neuroligins. MDGA1 binds NLGN2, but not NLGN1 or NLGN3, regulating inhibitory synaptogenesis *in vitro* and inhibitory synaptic transmission *in vivo* (Connor et al., 2016; Lee et al., 2013; Pettem et al., 2013). By contrast, though MDGA2 binds both NLGN1 and NLGN2 *in vitro*, controlling both excitatory and inhibitory synaptogenesis, *in vivo* MDGA2 knockdown impacts

excitatory but not inhibitory synaptic transmission (Connor et al., 2016). Our studies suggest a structural basis for this selectivity (Fig. 4c and 4d). MDGA1 Ig1 contacts 21 residues on NLGN2 within 5 Å; but they are virtually conserved between NLGN1, NLGN2, and NLGN3 (except for His^{279}), so they would unlikely encode selectivity (Fig. 4c, ***top***). However, directly adjacent to His^{279}, loop α7–β10 incorporates the large nine residue site B insert in NLGN1 (in NLGN2 equivalent residues would be Glu^{281} – Gly^{282}) (Fig. 4c, ***top***). This suggests that MDGA1 Ig1 may not be able to accommodate the site B insert, which we could also detect using purified proteins (Fig. 4d). To accommodate the site B insert, MDGA1 Ig1 loop β5–β6 (which is ordered in the MGDA1 structure but not in the complex with NLGN2, Fig. S5) would likely rearrange, acting perhaps as a gatekeeper. However, it is not yet clear why the Ig1 domain from MDGA2 can accommodate site B insert, while that from MDGA1 cannot, given that loop β5–β6 has a similar sequence in MDGA1 and MDGA2. Site A, the other alternative site insert found in neuroligins, located in loop β6–β7 (between Asp^{152} and Asp^{170}), is far away from the MDGA1 binding site, and unlikely affects the selectivity profile between MDGAs and NLGNs. Ig2 domain of MDGA1 may contribute to the neuroligin selectivity as well, because removal of the site B insert in NLGN1 is not sufficient to restore interaction with MDGA1 in cell-surface binding studies (Lee et al., 2013), though it does rescue binding between purified proteins to some extent (Fig. 4d). MDGA1 Ig2 contacts 18 residues of NLGN2 within 5 Å, of which fourteen are conserved between NLGN1, NLGN2, and NLGN3 and the other four residues are not (Asp^{442}, Ala^{403}, Ser^{404}, and Phe^{408}) (Fig. 4c, ***top***; Fig. S6). Though MDGAs display selectivity for different neuroligins, NLGN2 binds both MDGA1 and MDGA2. Cell-surface binding assays show that MDGA1 and MDGA2 bind a soluble NLGN2-F_c fusion protein with K_D ~ 7 nM and ~46 nM respectively (Pettem et al., 2013). This is supported by the high degree of sequence conservation on the surface of Ig1–Ig2 between the MDGAs (Fig. 4c, ***bottom***; Fig. S2). Sixteen residues from Ig1 contact NLGN2 within 5 Å (twelve of which are conserved), and seventeen residues from Ig2 (eleven of which are conserved), while the remaining semi-/non-conserved residues largely segregate to the periphery of the binding site (Fig. 4c, ***bottom***). The molecular selectivity may result from several semi-conserved substitutions rather than from one particular residue, and additional studies are needed to delve more deeply into the precise mechanism.

Discussion

A new family of synaptic organizers, MDGAs, has emerged that do not possess trans-adhesive function, rather play a regulatory role by modifying the trans-synaptic adhesion of two other proteins, neurexins and neuroligins. We determined that the first two Ig-domains of MDGA1 bind NLGN2 with nanomolar affinity in solution. The MDGA1 Ig1–Ig2 structure shows a rod-shaped array locked by an uncommon interdomain disulfide bond. The structure of the complex between MDGA1 Ig1–Ig2 and NLGN2 reveals two MDGA1 molecules bound to the NLGN2 dimer. Strikingly, each Ig1–Ig2 array spans the entire NLGN2 dimer because Ig1 and Ig2 bind to separate monomers. The binding of MDGA1 Ig1–Ig2 to NLGN2 is mediated by an extensive network of interactions composed of electrostatic interactions, hydrogen bonds and hydrophobic interactions. Mutagenesis of key residues at the binding interface confirms that the observed interface is physiologically

relevant. Ig1 interacts in part with the molecular surface of NLGN2 that is also used by neurexins to bind to neuroligins, thereby revealing the mechanism of regulatory action by MDGAs.

MDGA1 and NLGN2 subunits

The conformation of MDGA1 Ig1–Ig2 is remarkable because an uncommon interdomain disulfide bond between Ig1 and Ig2 rigidifies the tandem. By holding the two binding surfaces for NLGN2 aligned with respect to each other the conformational entropy is lowered which likely increases the binding affinity of MDGA1 Ig1–Ig2 for NLGN2. Strikingly, in the context of full-length MDGAs, Ig1–Ig2 was predicted to fold back on Ig3–Ig4 adopting a horseshoe-shaped configuration, as seen for example, in contactins, neurofascin, DCC (deleted in colorectal cancer) and L1 (Chen et al., 2013; Freigang et al., 2000; Liu et al., 2011; Schürmann et al. 2001). The horseshoe-shape was predicted to require 1) a 5–7 residue linker between Ig2 and Ig3, 2) a W-X-X-N/D motif on the C–C' turn in Ig4, and 3) a Gln in the Y-Q-C motif on strand F in Ig4 (Chen et al., 2013). While MDGA1 meets the first two criteria, the surface of Ig1–Ig2 that is predicted to bury itself against Ig3–Ig4 to form the horseshoe, is in fact the interaction site for NLGN2. Therefore, such a horseshoe-shaped arrangement of MDGA1 Ig1–Ig4, would preclude binding to neuroligins. Instead, we show that MDGA1 Ig1–Ig2 and MDGA1 Ig1–Ig4 both bind NLGN2 with nanomolar affinity (Fig. 1). In fact, we observed that the presence of Ig3 lowered the affinity of MDGA1 fragments towards NLGN2 approximately 10-fold. One explanation is that Ig3 can bend back to interact with Ig2, but that Ig4 has evolved to have a repulsive effect on Ig1, forcing the MDGA1 Ig1–Ig4 array to adopt an extended conformation thereby promoting efficient interaction with NLGN2.

The MDGA1 Ig1–Ig2 tandem spans the entire NLGN2 dimer suggesting that MDGA1 might stabilize the NLGN2 dimer. Such stabilization would be important because dimer formation is essential for neuroligin function (Shipman & Nicoll, 2012). When MDGA1 latches onto NLGN2, the concave surface of MDGA1 Ig2 interacts with the dimerization domain of NLGN2, binding helix α14 and burying helix α13 deeply in its cleft. Helix α13 forms part of an EF-hand motif, a structural feature that had been noted in neuroligins, but for which no function could be assigned yet (Arac et al., 2007). However, it is known that NLGN2 can also form heterodimers with NLGN3, though their function is not known (Budreck & Scheiffele, 2007; Poulopoulos et al. 2012), and the residues mediating dimerization are virtually conserved across mammalian neuroligins (Koenhke et al., 2008). Because NLGN3 does not appear to bind to MDGA1 (Lee et al., 2013), it is therefore possible that the NLGN2:NLGN3 heterodimers bypass regulation by MDGAs because the Ig-tandem is not able to bind neuroligin heterodimers efficiently, suggesting thereby also a unique function for them.

MDGA1 Ig1–Ig2:NLGN2 complex

The MDGA1 and NLGN2 molecules dock together largely as preformed entities in the crystal structure. The Ig1–Ig2 tandem maintains a very similar configuration alone compared to in complex with NLGN2 with the exception of two loops (see Fig. S5). First, in Ig1, loop β5–β6 (in particular Thr^{75}-Gln^{84}) is ordered in the unbound structure, but disordered in

complex; this loop would clash with NLGN2 loops α7–β10 (Ser^{280}-Leu^{283}) and α11–β11 (Leu^{374}-Tyr^{376}). Second, in Ig2, the loop β12–β13 (in particular Pro^{189}-Gln^{193}) moves outwards to widen the concave surface of this domain, to accommodate the insertion of NLGN2 helix α13. By contrast, NLGN2 does not appear to undergo any large scale conformational rearrangements when MDGA1 is bound.

Molecular mechanism of MDGA1 regulatory function

The binding site of neurexin on NLGN1 and NLGN4 was identified by determining several crystals structures, and mutational analyses have confirmed the interaction site (Arac et al., 2007; Chen et al., 2008; Fabrichny et al., 2008; Graf et al., 2006; Ko et al., 2009; Leone et al., 2010; Reissner et al., 2008). The neuroligin cholinesterase module uses the edge of its central β-sheet to bind loops at the rim of the β-sandwich and a Ca^{2+}-binding site that are located close together in the neurexin LNS domain (L6 in neurexin 1α and the single L domain in neurexin 1β). Electrostatic interactions, hydrogen bonds, a Ca^{2+}-ion and a key water molecule comprise the interface, supporting nanomolar affinity between the neuroligins (NLGN1 and NLGN4) and neurexin 1β. While there is significant overlap between the neuroligin residues that bind MDGA1 and those that bind neurexin, the two binding sites do not appear to be identical. Of the 16 NLGN1 residues that bind neurexin within 5 Å, only 11 of these are identical with NLGN2 residues that bind the Ig1 domain of MDGA1 (Fig. S6). It is curious that cells expressing NLGN2 and MDGA1, respectively, do not bind each other in co-culture (as assessed by cell aggregation) which would require *trans*-interaction, while cells expressing neuroligins and neurexins do. The soluble extracellular domain of MDGA1 does bind to cell surface NLGN2 (Lee et al., 2013), which suggests that perhaps the manner in which MDGA1 is presented to NLGN2 in the synaptic cleft also plays a role in steering the interactions and limiting binding to *cis* interactions. In future, it will be important to more precisely delineate the molecular interactions between neuroligins, MDGAs, neurexins, and the protein networks that they organize in the synaptic cleft, because manipulating their interactions selectively could open up new therapeutic avenues to treat their associated neuropsychiatric disorders (Rudenko et al., 2017).

STAR Methods

EXPERIMENTAL MODEL AND SUBJECT DETAILS

cDNAs used for expression of recombinant proteins were of human, rat and bovine origin. The genes encoding the respective proteins were cloned in the pFastbac vector and expressed using baculovirus mediated overexpression.

METHOD DETAILS

Protein Expression and Purification—The extracellular domain of human MDGA1 (NM_153487) with a C-terminal linker and hexahistidine tag was cloned into the pFastbac vector. A panel of constructs were made: MDGA1 C1 (Ig1-MAM domain; Y^{22}-Q^{920}), MDGA1 C2 (Ig1–Ig3; Y^{22}-K^{330}), MDGA1 C4 (Ig1–Ig4; Y^{22}-I^{433}), MDGA1 C5 (Ig1; Y^{22}-D^{130}), MDGA1 C7 (Ig3; A^{238}-K^{330}), MDGA1 C8 (Ig1–Ig2; Y^{22}-T^{237}), MDGA1 C9 (Ig2–Ig3; E^{131}-K^{330}). The extracellular domain encoding rat NLGN2 (Val^{43}-His^{612}; NM_053992 containing the site A insert), human NLGN1 (no A insert, but with and without site B; D^{52}-

N^{637}; BC032555) and bovine n1α L5L6 (A^{911}-S^{1339}; NM_174404) were made similarly. In addition, a series of mutants were made based on MDGA1 C8 and NLGN2.

The proteins were produced using baculovirus-mediated overexpression in HighFive cells with Insect-XPRESS+L-Glutamine medium (Lonza) at 28 °C over an infection course of 70–72 hr. The medium containing the secreted proteins and protease inhibitors (pepstatin, PMSF, leupeptin) was concentrated. For MDGA1 proteins, concentrated media was dialyzed overnight in 25 mM sodium phosphate pH 8.0, 500 mM NaCl, then subjected to Ni-NTA affinity chromatography (Invitrogen), followed by dialysis into 25 mM Tris pH 8.0, 50 mM NaCl and ion-exchange chromatography (Mono S; GE Healthcare) eluting with a NaCl gradient. As a final step, MDGA1 proteins were purified by size exclusion chromatography (HiLoad Superdex-200 16/60; GE Healthcare) in 10 mm HEPES pH 8.0, 50 mM NaCl.

To purify NLGN2, as well as NLGN1 (+/− siteB), concentrated media was dialyzed overnight in 20 mM Tris pH 8.0, 500 mM NaCl, then subjected to Ni-NTA affinity chromatography (Invitrogen), followed by dialysis into 20 mM Bis-Tris pH 7.0, 100 mM NaCl and ion-exchange chromatography (Mono Q; GE Healthcare) eluting with a NaCl gradient. As a final step, NLGN2 proteins were purified by size exclusion chromatography (HiLoad Superdex-200 16/60; GE Healthcare) in 10 mm HEPES pH 8.0, 150 mM NaCl, while NLGN1 (+/− siteB) were purified in 10 mm Tris pH 8.0, 150 mM NaCl. Purified proteins in their gel filtration buffers were concentrated to 10 mg/ml and stored as flash-frozen aliquots at −80 °C.

Bovine n1α L5L6 was produced as previous described (Chen et al., 2011) also using baculovirus mediated over-expression in HighFive cells. Medium containing the secreted proteins was concentrated, dialyzed in 25 mM sodium phosphate pH 8.0 and 500 mM NaCl, and then subjected to Ni-NTA chromatography followed by dialysis in 25 mM Tris pH 8.0 and 50 mM NaCl and ion exchange chromatography (Mono Q, GE Healthcare). As a final step, n1α L5L6 was purified by size exclusion chromatography (HiLoad Superdex-200 16/60; GE Healthcare) in 25 mm Tris pH 8.0, 100 mM NaCl.

Protein Labeling—MDGA1, the panel of MDGA1 fragments, the panel of MDGA1 C8 mutants and n1α L5L6 were labeled using OneQuant (5/6)-TAMRA-SE fluorescent probe (G-Biosciences). For labeling, 100 μM protein and 1000 μM fluorescent probe, dissolved in 100 % DMSO (Sigma), were mixed in 10 mM HEPES pH 7.5 in a reaction volume of 500 μL. The reaction mixture was incubated at room temperature for 2 hr protected from light. The labeled proteins were separated from unbound probe using SpinOUT GT-600 columns (G-Biosciences).

Binding Assay—We developed a fluorescence polarization assay to measure the binding affinity between different TAMRA-labeled proteins and NLGN2. Prior to use, TAMRA (TMR) labeled proteins were diluted in 20 mM HEPES pH 7.5, 25 mM NaCl. A concentration series of 0–500 nM NLGN2 with a fixed concentration of 30 nM TMR-labeled protein in 20 mM HEPES pH 7.5, 25 mM NaCl was made in 96-well flat bottom black assay plates (Corning-3991) using 200 μl/well. To measure the interaction of TMR-MDGA1 C8 with NLGN2, NLGN1(+ site B) and NLGN1(− site B), concentration series

containing 0 – 125 nM neuroligins were made in 20 mm HEPES pH 7.5, 75 mM NaCl with 30 nM TMR-labeled protein added. After incubation at room temperature for 15–20 min, fluorescence polarization was measured using a Pherastar plate reader (BMG Labs) at 25 °C, with excitation at 540 nm, emission at 590 nm, 100 flashes per well, and the target set to 50 mP for the TMR-labeled tracer by adjusting the gain on a well with 30 nM TAMRA in H_2O. Data were processed using Prism 6.0 (GraphPad Software), fitting the binding curves to a 'One Site-Total Binding' model. Each data point represents the mean of triplicates, and the error bar represents the standard deviation. The fluorescence polarization observed for 30 nM TMR-labeled tracer alone was set as the baseline value and subtracted from the values measured for 30 nM TMR-tracer in the presence of increasing amounts of NLGN2.

Competitive Binding Assay—To measure the competition of MDGA1 and neurexin for NLGN2 a modified FP-assay was used. First, the MDGA1 Ig1–Ig2:NLGN2 complex was made by mixing 5 nM TMR-MDGA1 C8 and 100 nM NLGN2 in 10 mM HEPES pH 7.5, 50 mM NaCl, 1 mM $CaCl_2$ and 0.01% Triton X-100. Subsequently, the complex and n1α L5L6 was dispensed in a 96-well flat bottom black assay plate (Corning-3991) so that each well received a final volume of 100 µl complex containing a serial dilution of n1α L5L6; separately wells with TMR-MDGA1 C8:NLGN2 but no n1α L5L6 were also taken along to form a final concentration range of 0 – 4000 nM n1α L5L6. Plates were incubated at room temperature for 1 hr with gentle shaking; then the fluorescence polarization was measured using a Pherastar plate reader (BMG Labs) at 25 °C, with excitation at 540 nm, emission at 590 nm, 200 flashes per well, and the target set to 50 mP for the TMR-labeled tracer by adjusting the gain on a well with 5 nM TAMRA in H_2O. Data were processed as above. Each data point represents the mean of duplicates, and the error bar represents the standard deviation.

Crystallization—Crystals of MDGA1 C8 (Ig1–Ig2) were grown at 20 °C by mixing 2.5 µl of protein at 1.5 mg/ml and 2.5 µl of reservoir solution (1.5 M ammonium sulfate, 3.72% (v/v) 2-propanol, 25% (v/v) glycerol) in a hanging drop setup. Crystals were harvested directly from the crystallization drops and flash cooled. The crystals exhibit the symmetry of space group I23 with unit cell dimensions a=b=c=139.07 Å, α=β=γ=90° and diffract to 2.76 Å. To grow crystals of the MDGA1 Ig1–Ig2:NLGN2 complex, the two proteins were mixed (NLGN2 at ~3.9 mg/ml and MDGA1 C8 at ~2.4 mg/ml, respectively, to achieve a ratio of 60:90 µM) in 10 mM HEPES pH 8.0, 50 mM NaCl and incubated at room temperature for ~1 hr. Crystals were obtained at 20 °C by mixing 2.5 µl of protein complex and 2.5 µl of reservoir solution (0.03 M $NaNO_3$, 0.03 M Na_2HPO_4, 0.03 M $(NH_4)_2SO_4$, 0.05 M HEPES pH 7.5, 0.05 M MOPS pH 7.5, 12 % (v/v) ethylene glycol, 9 % (w/v) PEG 8000) in a hanging drop setup. Crystals were cryo-protected in reservoir solution containing 20% (v/v) glycerol and flash-cooled. The crystals exhibit the symmetry of space group P1 with unit cell dimensions a=103.12 Å, b=97.18 Å, c=190.51 Å, α=95.52°, β=80.97°, γ=88.71° and diffract to 4.1 Å. Diffraction datasets were collected at the Advanced Photon Source (LS-CAT, SBC-CAT and IMCA-CAT). Data were processed with HKL2000 (Otwinowski & Minor, 1997) and data statistics are given in Table 1.

Structure Determination of MDGA1 Ig1–Ig2—The structure of MDGA1 Ig1–Ig2 was determined by molecular replacement using the program MrBUMP (Keegan and Winn, 2008) using the coordinates of the insect immune protein hemolin (PDB ID: 1BIH; Su et al., 1998) as search model. Model building was iteratively carried out with the program Coot (Emsley et al., 2010) interspersed with refinement using the Phenix program package (Adams et al., 2010). The refined model consists of 198 residues (Tyr^{22}–Thr^{234}) with good geometry (95.8 % in the preferred region (182 residues), 4.2 % in the allowed region (8 residues) and no outliers of the Ramachandran plot) as well as three sulfate ions, one chloride ion and ten water molecules. Electron density for the residues Asn^{90} (loop β5–β6), Ser^{141}-Glu^{150} (loop β9–β10) and His^{178}-Asp^{181} (loop β11–β12) is poor or missing and these residues were not incorporated in the model.

Structure determination of the MDGA1 Ig1–Ig2:NLGN2 complex—The structure of the MDGA1 Ig1–Ig2-NLGN2 complex was determined by molecular replacement using the coordinates of MDGA1 Ig1–Ig2 (described herein) and NLGN2 (PDB ID: 3BL8; Koenhke et al., 2008) as search models with the program Phaser (McCoy et al., 2007). An initial solution placed three NLGN2 dimers and four MDGA1 molecules. Spurious density indicated the presence of two more MDGA1 molecules, which upon six-fold averaging of the density with RAVE (Kleywegt and Jones,1994) and DM (Cowtan, 1994) could be sequentially added to the model, completing the packing of three NLGN2 dimers each with two MDGA1 Ig1–Ig2 molecules bound. For model building, unsharpened, sharpened, as well as averaged maps were inspected, unambiguously revealing the interactions between NLGN2 and MDGA1. Electron density for the main-chain trace of the NLGN2 monomers A, B, C, D, and E is clear, while monomer F is less well resolved suggesting disorder. While MDGA1 Ig1–Ig2 molecules G and H show clear density for both Ig1 and Ig2 domains, in molecules J, K, and L the Ig2 has better-resolved electron density compared to Ig1 domain suggesting some disorder in the latter; molecule I is not well resolved. Therefore, model building was carried out only for molecule A (NLGN2) and molecule G (MDGA1); the other molecules were generated using non-crystallographic (NCS) symmetry and six-fold local NCS restraints were used for refinement with Refmac (Murshudov et al., 2011), which led to a steadily decreasing R_{free} in parallel with R_{work} as the completeness of the model increased with model building/refinement cycles. To accommodate for the limited resolution of the diffraction data, an overall B-factor was refined but not applied to the model and side chains were incorporated according to the higher resolution structures of the individual components, NLGN2 and MDGA1 Ig1–Ig2. The refined model consists of 4266 residues in total with each complex containing two NL2 monomers (a.a. 51–609) and two MDGA1 Ig1–Ig2 fragments (a.a. 24–234) (with good geometry (84.1% in favorable region, 13.8% in the allowed region and 2.1% outliers in the Ramachandran plot). Electron density for the residues N^{59}-E^{61}, L^{155}-D^{173}, G^{491}-A^{496}, I^{558}-K^{561} in NLGN2 (molecule A) and H^{65}-P^{66}, T^{75}-Q^{84}, N^{90}, S^{141}-K^{151}, H^{178}-D^{181} in MDGA1 (molecule G) is poor, and these residues were not incorporated in the model.

Structure analysis—Analysis of the structure was carried out using molecules, A and B for NLGN2, and G and H for MDGA1 Ig1–Ig2. Secondary structure elements for MDGA1 Ig1–Ig2 were calculated by DSSP (Kabsch and Sander, 1983). Buried-surface calculations

were performed by PDBe PISA (Krissinel and Henrick, 2007). Interactions between MDGA1 Ig1–Ig2 and NLGN2 were assessed using NCONT (CCP4, Winn et al., 2011) to identify distances less than 5 Å. Sequence homology comparisons were carried out with the following sequences: NLGN2 (human, AAM46111.1; bovine, NP_001178171.1; rat, AAA97870.1; mouse, EDL12455.1), NLGN1 (human, ADB12633.1; bovine, NP_001192902.1; rat, NP_446320.1; mouse, NP_619607.2), NLGN3 (human, ADB12634.1; bovine, AAI23786.1; rat, AAA97871.1; mouse, AAI50774.1), MDGA1 (human, NM_153487.3; bovine, NP_001179811.1; rat, NP_001101088.1; mouse, ABG78614.1) and MDGA2 (human, NP_001106970.3; bovine, XP_015320545.1; rat, NP_954890.1; mouse, AAI37903.1). The following groups of residues were considered semi-conserved (I, V, L, M); (F, Y, W); (K, R, H), (D, E, N, Q); (G, A, S, T); (C) and (P). Figures were prepared using the PyMol Molecular Graphics System, Schrödinger, LLC.

QUANTIFICATION AND STATISTICAL ANALYSIS

Fluorescence polarization data was processed using Prism 6.0 (GraphPad Software). For fluorescence polarization experiments, values are shown as mean ± standard deviation (described in Method Details).

DATA AND SOFTWARE AVAILABILITY

The coordinates for MDGA1 Ig1–Ig2 and MDGA1 Ig1–Ig2:NLGN2 complex reported in this paper have been deposited in the protein data bank with accession number 5V5W and 5V5V respectively.

Supplementary Material

Refer to Web version on PubMed Central for supplementary material.

Acknowledgments

Fang Chen is thanked for preliminary studies. This work was funded by NIMH (R01MH077303), a UT BRAIN Award, the Brain and Behavior Research Foundation and the SCSB at UTMB. The Advanced Photon Source (LS-CAT, SBC-CAT and IMCA-CAT) are thanked for access to synchrotron radiation.

References

Adams PD, Afonine PV, Bunkoczi G, Chen VB, Davis IW, Echols N, Headd JJ, Hung LW, Kapral GJ, Grosse-Kunstleve RW, et al. PHENIX: a comprehensive Python-based system for macromolecular structure solution. Acta Crystallogr D Biol Crystallogr. 2010; 66:213–221. [PubMed: 20124702]

Arac D, Boucard AA, Ozkan E, Strop P, Newell E, Sudhof TC, Brunger AT. Structures of neuroligin-1 and the neuroligin-1/neurexin-1 beta complex reveal specific protein-protein and protein-Ca2+ interactions. Neuron. 2007; 56:992–1003. [PubMed: 18093522]

Bemben MA, Shipman SL, Nicoll RA, Roche KW. The cellular and molecular landscape of neuroligins. Trends Neurosci. 2015; 38:496–505. [PubMed: 26209464]

Bena F, Bruno DL, Eriksson M, van Ravenswaaij-Arts C, Stark Z, Dijkhuizen T, Gerkes E, Gimelli S, Ganesamoorthy D, Thuresson AC, et al. Molecular and clinical characterization of 25 individuals with exonic deletions of NRXN1 and comprehensive review of the literature. Am J Med Genet B Neuropsychiatr Genet. 2013; 162B:388–403. [PubMed: 23533028]

Boucard AA, Chubykin AA, Comoletti D, Taylor P, Sudhof TC. A splice code for trans-synaptic cell adhesion mediated by binding of neuroligin 1 to alpha- and beta-neurexins. Neuron. 2005; 48:229–236. [PubMed: 16242404]

Bourgeron T. Current knowledge on the genetics of autism and propositions for future research. C R Biol. 2016; 339:300–307. [PubMed: 27289453]

Bucan M, Abrahams BS, Wang K, Glessner JT, Herman EI, Sonnenblick LI, Alvarez Retuerto AI, Imielinski M, Hadley D, Bradfield JP, et al. Genome-wide analyses of exonic copy number variants in a family-based study point to novel autism susceptibility genes. PLoS Genet. 2009; 5:e1000536. [PubMed: 19557195]

Budreck EC, Scheiffele P. Neuroligin-3 is a neuronal adhesion protein at GABAergic and glutamatergic synapses. Eur J Neurosci. 2007; 26:1738–1748. [PubMed: 17897391]

Chen F, Venugopal V, Murray B, Rudenko G. The structure of neurexin 1alpha reveals features promoting a role as synaptic organizer. Structure. 2011; 19:779–789. [PubMed: 21620716]

Chen Q, Sun X, Zhou XH, Liu JH, Wu J, Zhang Y, Wang JH. N-terminal horseshoe conformation of DCC is functionally required for axon guidance and might be shared by other neural receptors. J Cell Sci. 2013; 126:186–195. [PubMed: 23038776]

Chen X, Liu H, Shim AH, Focia PJ, He X. Structural basis for synaptic adhesion mediated by neuroligin-neurexin interactions. Nat Struct Mol Biol. 2008; 15:50–56. [PubMed: 18084303]

Chih B, Gollan L, Scheiffele P. Alternative splicing controls selective trans-synaptic interactions of the neuroligin-neurexin complex. Neuron. 2006; 51:171–178. [PubMed: 16846852]

Chubykin AA, Atasoy D, Etherton MR, Brose N, Kavalali ET, Gibson JR, Sudhof TC. Activity-dependent validation of excitatory versus inhibitory synapses by neuroligin-1 versus neuroligin-2. Neuron. 2007; 54:919–931. [PubMed: 17582332]

Connor SA, Ammendrup-Johnsen I, Chan AW, Kishimoto Y, Murayama C, Kurihara N, Tada A, Ge Y, Lu H, Yan R, et al. Altered Cortical Dynamics and Cognitive Function upon Haploinsufficiency of the Autism-Linked Excitatory Synaptic Suppressor MDGA2. Neuron. 2016; 91:1052–1068. [PubMed: 27608760]

Cowtan K. Joint CCP4 and ESF-EACBM Newsletter on Protein Crystallography. 1994; 31:34–38.

Emsley P, Lohkamp B, Scott WG, Cowtan K. Features and development of Coot. Acta Crystallogr D Biol Crystallogr. 2010; 66:486–501. [PubMed: 20383002]

Fabrichny IP, Leone P, Sulzenbacher G, Comoletti D, Miller MT, Taylor P, Bourne Y, Marchot P. Structural analysis of the synaptic protein neuroligin and its beta-neurexin complex: determinants for folding and cell adhesion. Neuron. 2007; 56:979–991. [PubMed: 18093521]

Freigang J, Proba K, Leder L, Diederichs K, Sonderegger P, Welte W. The crystal structure of the ligand binding module of axonin-1/TAG-1 suggests a zipper mechanism for neural cell adhesion. Cell. 2000; 101:425–433. [PubMed: 10830169]

Futai K, Doty CD, Baek B, Ryu J, Sheng M. Specific trans-synaptic interaction with inhibitory interneuronal neurexin underlies differential ability of neuroligins to induce functional inhibitory synapses. J Neurosci. 2013; 33:3612–3623. [PubMed: 23426688]

Gibson JR, Huber KM, Sudhof TC. Neuroligin-2 deletion selectively decreases inhibitory synaptic transmission originating from fast-spiking but not from somatostatin-positive interneurons. J Neurosci. 2009; 29:13883–13897. [PubMed: 19889999]

Graf ER, Kang Y, Hauner AM, Craig AM. Structure function and splice site analysis of the synaptogenic activity of the neurexin-1 beta LNS domain. J Neurosci. 2006; 26:4256–4265. [PubMed: 16624946]

Hagihara Y, Saerens D. Engineering disulfide bonds within an antibody. Biochim Biophys Acta. 2014; 1844:2016–2023. [PubMed: 25038323]

Ishikawa T, Gotoh N, Murayama C, Abe T, Iwashita M, Matsuzaki F, Suzuki T, Yamamoto T. IgSF molecule MDGA1 is involved in radial migration and positioning of a subset of cortical upper-layer neurons. Dev Dyn. 2011; 240:96–107. [PubMed: 21104742]

Kabsch W, Sander C. Dictionary of protein secondary structure: pattern recognition of hydrogen-bonded and geometrical features. Biopolymers. 1983; 22:2577–2637. [PubMed: 6667333]

Kahler AK, Djurovic S, Kulle B, Jonsson EG, Agartz I, Hall H, Opjordsmoen S, Jakobsen KD, Hansen T, Melle I, et al. Association analysis of schizophrenia on 18 genes involved in neuronal migration:

MDGA1 as a new susceptibility gene. Am J Med Genet B Neuropsychiatr Genet. 2008; 147B: 1089–1100. [PubMed: 18384059]

Keegan RM, Winn MD. MrBUMP: an automated pipeline for molecular replacement. Acta Crystallogr D Biol Crystallogr. 2008; 64:119–124. [PubMed: 18094475]

Kleywegt, GJ., Jones, TA. Halloween … Masks and Bones. In: Bailey, S.Hubbard, R., Waller, D., editors. From First Map to Final Model. SERC Daresbury Laboratory; 1994. p. 59-66.

Ko J, Zhang C, Arac D, Boucard AA, Brunger AT, Sudhof TC. Neuroligin-1 performs neurexin-dependent and neurexin-independent functions in synapse validation. The EMBO J. 2009; 28:3244–3255. [PubMed: 19730411]

Koehnke J, Jin X, Budreck EC, Posy S, Scheiffele P, Honig B, Shapiro L. Crystal structure of the extracellular cholinesterase-like domain from neuroligin-2. Proc Natl Acad Sci USA. 2008; 105:1873–1878. [PubMed: 18250328]

Krissinel E, Henrick K. Inference of macromolecular assemblies from crystalline state. J Mol Biol. 2007; 372:774–797. [PubMed: 17681537]

Lee E, Lee J, Kim E. Excitation/Inhibition Imbalance in Animal Models of Autism Spectrum Disorders. Biol Psychiatry. 2016; doi: 10.1016/j.biopsych.2016.05.011

Lee K, Kim Y, Lee SJ, Qiang Y, Lee D, Lee HW, Kim H, Je HS, Sudhof TC, Ko J. MDGAs interact selectively with neuroligin-2 but not other neuroligins to regulate inhibitory synapse development. Proc Natl Acad Sci USA. 2013; 110:336–341. [PubMed: 23248271]

Leone P, Comoletti D, Ferracci G, Conrod S, Garcia SU, Taylor P, Bourne Y, Marchot P. Structural insights into the exquisite selectivity of neurexin/neuroligin synaptic interactions. The EMBO J. 2010; 29:2461–2471. [PubMed: 20543817]

Levinson JN, Chery N, Huang K, Wong TP, Gerrow K, Kang R, Prange O, Wang YT, El-Husseini A. Neuroligins mediate excitatory and inhibitory synapse formation: involvement of PSD-95 and neurexin-1beta in neuroligin-induced synaptic specificity. J Biol Chem. 2005; 280:17312–17319. [PubMed: 15723836]

Li J, Liu J, Feng G, Li T, Zhao Q, Li Y, Hu Z, Zheng L, Zeng Z, He L, et al. The MDGA1 gene confers risk to schizophrenia and bipolar disorder. Schizophr Res. 2011; 125:194–200. [PubMed: 21146959]

Litwack ED, Babey R, Buser R, Gesemann M, O'Leary DD. Identification and characterization of two novel brain-derived immunoglobulin superfamily members with a unique structural organization. Mol Cell Neurosci. 2004; 25:263–274. [PubMed: 15019943]

Liu H, Focia PJ, He X. Homophilic adhesion mechanism of neurofascin, a member of the L1 family of neural cell adhesion molecules. J Biol Chem. 2011; 286:797–805. [PubMed: 21047790]

Loh KH, Stawski PS, Draycott AS, Udeshi ND, Lehrman EK, Wilton DK, Svinkina T, Deerinck TJ, Ellisman MH, Stevens B, et al. Proteomic Analysis of Unbounded Cellular Compartments: Synaptic Clefts. Cell. 2016; 166:1295–1307. [PubMed: 27565350]

McCoy AJ, Grosse-Kunstleve RW, Adams PD, Winn MD, Storoni LC, Read RJ. Phaser crystallographic software. J Appl Crystallogr. 2007; 40:658–674. [PubMed: 19461840]

Murshudov GN, Skubak P, Lebedev AA, Pannu NS, Steiner RA, Nicholls RA, Winn MD, Long F, Vagin AA. REFMAC5 for the refinement of macromolecular crystal structures. Acta Crystallogr D Biol Crystallogr. 2011; 67:355–367. [PubMed: 21460454]

Otwinowski Z, Minor W. Processing of X-ray diffraction data collected in oscillation mode. Methods Enzymol. 1997; 276:307–326.

Pettem KL, Yokomaku D, Takahashi H, Ge Y, Craig AM. Interaction between autism-linked MDGAs and neuroligins suppresses inhibitory synapse development. J Cell Biol. 2013; 200:321–336. [PubMed: 23358245]

Poulopoulos A, Soykan T, Tuffy LP, Hammer M, Varoqueaux F, Brose N. Homodimerization and isoform-specific heterodimerization of neuroligins. Biochem J. 2012; 446:321–330. [PubMed: 22671294]

Reissner C, Klose M, Fairless R, Missler M. Mutational analysis of the neurexin/neuroligin complex reveals essential and regulatory components. Proc Natl Acad Sci USA. 2008; 105:15124–15129. [PubMed: 18812509]

Reissner C, Runkel F, Missler M. Neurexins. Genome Biol. 2013; 14:213. [PubMed: 24083347]

Rudenko G. Dynamic Control of Synaptic Adhesion and Organizing Molecules in Synaptic Plasticity. Neur Plast. 2017; 2017 6526151.

Schreiner D, Nguyen TM, Russo G, Heber S, Patrignani A, Ahrne E, Scheiffele P. Targeted combinatorial alternative splicing generates brain region-specific repertoires of neurexins. Neuron. 2014; 84:386–398. [PubMed: 25284007]

Schreiner D, Simicevic J, Ahrne E, Schmidt A, Scheiffele P. Quantitative isoform-profiling of highly diversified recognition molecules. Elife. 2015; 4:e07794. [PubMed: 25985086]

Schürmann G, Haspel J, Grumet M, Erickson HP. Cell adhesion molecule L1 in folded (horseshoe) and extended conformations. Mol Biol Cell. 2001; 12:1765–1773. [PubMed: 11408583]

Shipman SL, Nicoll RA. Dimerization of postsynaptic neuroligin drives synaptic assembly via transsynaptic clustering of neurexin. Proc Natl Acad Sci USA. 2012; 109:19432–19437. [PubMed: 23129658]

Su XD, Gastonia LN, Vaughn DE, Faye I, Poon P, Bjorkman PJ. Crystal structure of hemolin: a horseshoe shape with implications for homophilic adhesion. Science. 1998; 281:991–995. [PubMed: 9703515]

Sun C, Cheng MC, Qin R, Liao DL, Chen TT, Koong FJ, Chen G, Chen CH. Identification and functional characterization of rare mutations of the neuroligin-2 gene (NLGN2) associated with schizophrenia. Hum Mol Genet. 2011; 20:3042–3051. [PubMed: 21551456]

Takeuchi A, O'Leary DD. Radial migration of superficial layer cortical neurons controlled by novel Ig cell adhesion molecule MDGA1. J Neurosci. 2006; 26:4460–4464. [PubMed: 16641224]

Treutlein B, Gokce O, Quake SR, Sudhof TC. Cartography of neurexin alternative splicing mapped by single-molecule long-read mRNA sequencing. Proc Natl Acad Sci USA. 2014; 111:E1291–1299. [PubMed: 24639501]

Varoqueaux F, Jamain S, Brose N. Neuroligin 2 is exclusively localized to inhibitory synapses. Eur J Cell Biol. 2004; 83:449–456. [PubMed: 15540461]

Winn MD, Ballard CC, Cowtan KD, Dodson EJ, Emsley P, Evans PR, Keegan RM, Krissinel EB, Leslie AG, McCoy A, et al. Overview of the CCP4 suite and current developments. Acta Crystallogr D Biol Crystallogr. 2011; 67:235–242. [PubMed: 21460441]

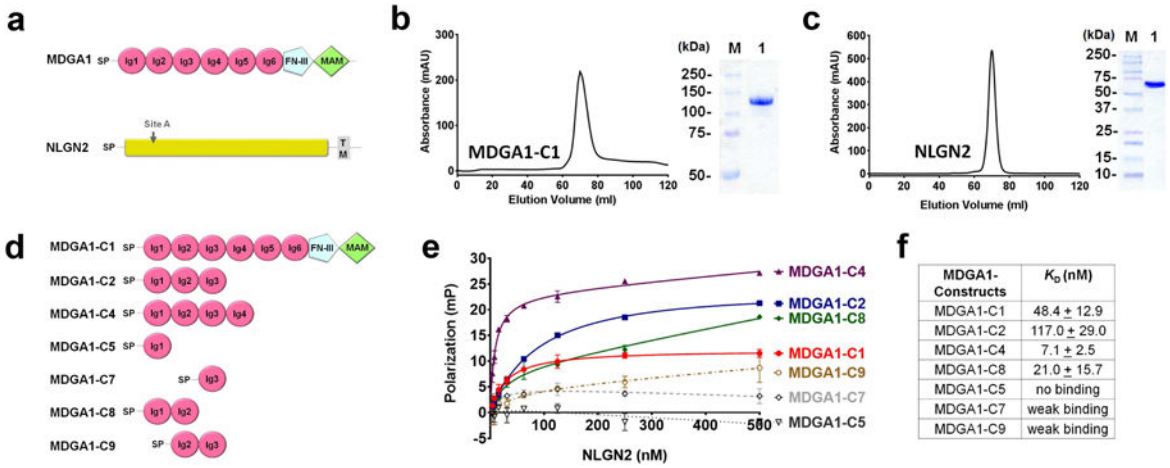

MDGA1-Constructs	K_D (nM)
MDGA1-C1	48.4 ± 12.9
MDGA1-C2	117.0 ± 29.0
MDGA1-C4	7.1 ± 2.5
MDGA1-C8	21.0 ± 15.7
MDGA1-C5	no binding
MDGA1-C7	weak binding
MDGA1-C9	weak binding

Figure 1. MDGA1 and NLGN2

(A) Domain structure of MDGA1 and NLGN2. Signal peptide (SP), immunoglobulin domain (Ig), fibronectin type III domain (FN-III), ‘meprin, A-5 protein, and receptor protein-tyrosine phosphatase μ′ domain (MAM), transmembrane segment (TM). The NLGN2 site A insert is indicated. **(B)** MDGA1 extracellular domain as shown by size exclusion chromatography (left) and SDS-PAGE (right). **(C)** NLGN2 extracellular domain as shown by size exclusion chromatography (left) and SDS-PAGE (right). **(D)** Domain structure of the MDGA1 fragments. **(E)** Representative FP-binding assays showing the interaction between the NLGN2 ectodomain and TAMRA-labeled MDGA1 fragments. Data points are in triplicate, and error bars indicate the standard deviation. **(F)** Calculated K_D values averaged over two independent experiments carried out on separate days (mean ± standard deviation).

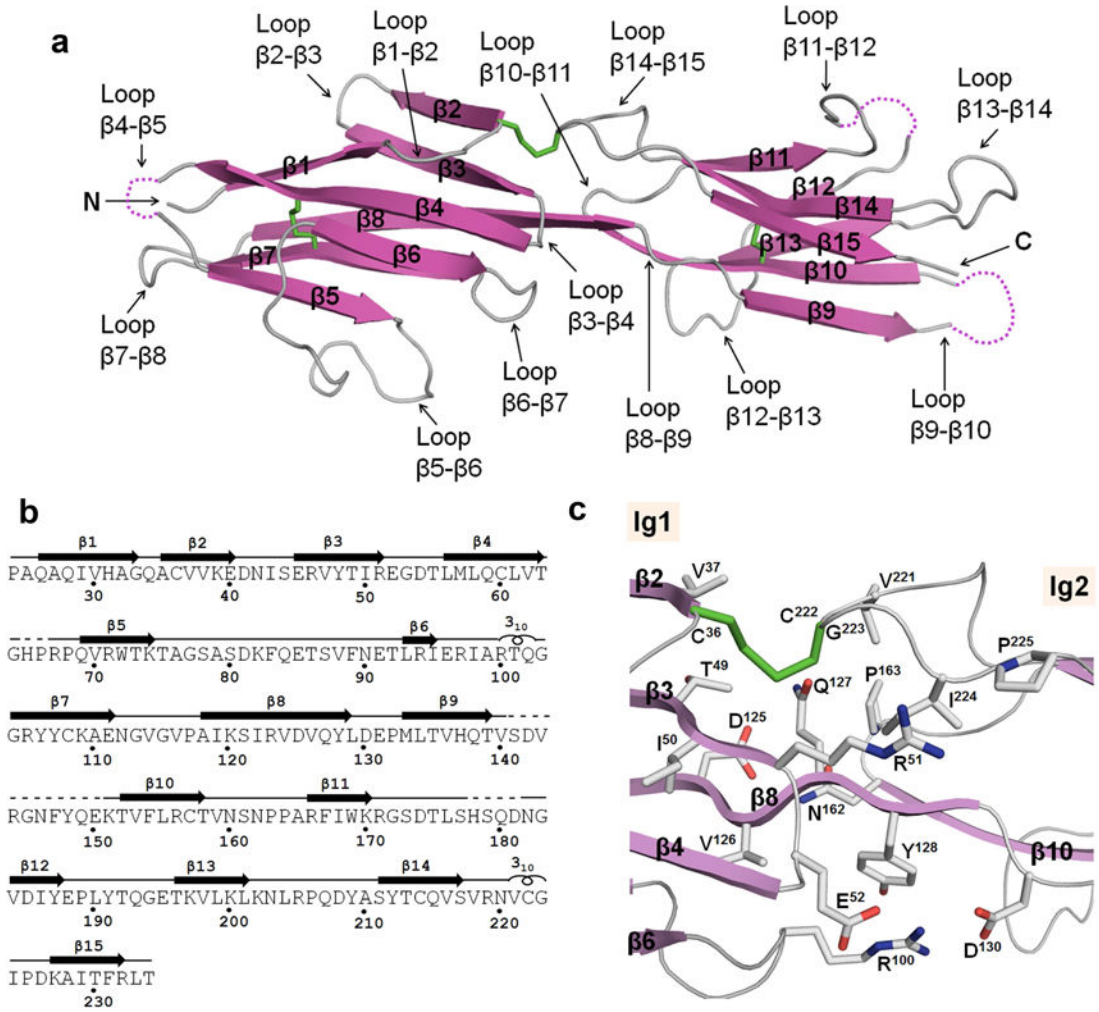

Figure 2. Crystal structure of MDGA1 Ig1–Ig2

(A) Ribbon diagram of MDGA1 Ig1–Ig2. For Ig2 the lettered naming convention is: β9/A, β10/B, β11/C, β12/D, β13/E, β14/F, and β15/G. **(B)** Secondary structure assignment as calculated by DSSP. **(C)** Close-up of the interface between MDGA1 Ig1 and Ig2. Select side chains are shown in ball-and-stick representation (nitrogen, blue; oxygen, red; carbon, grey; disulfide bonded residues, green).

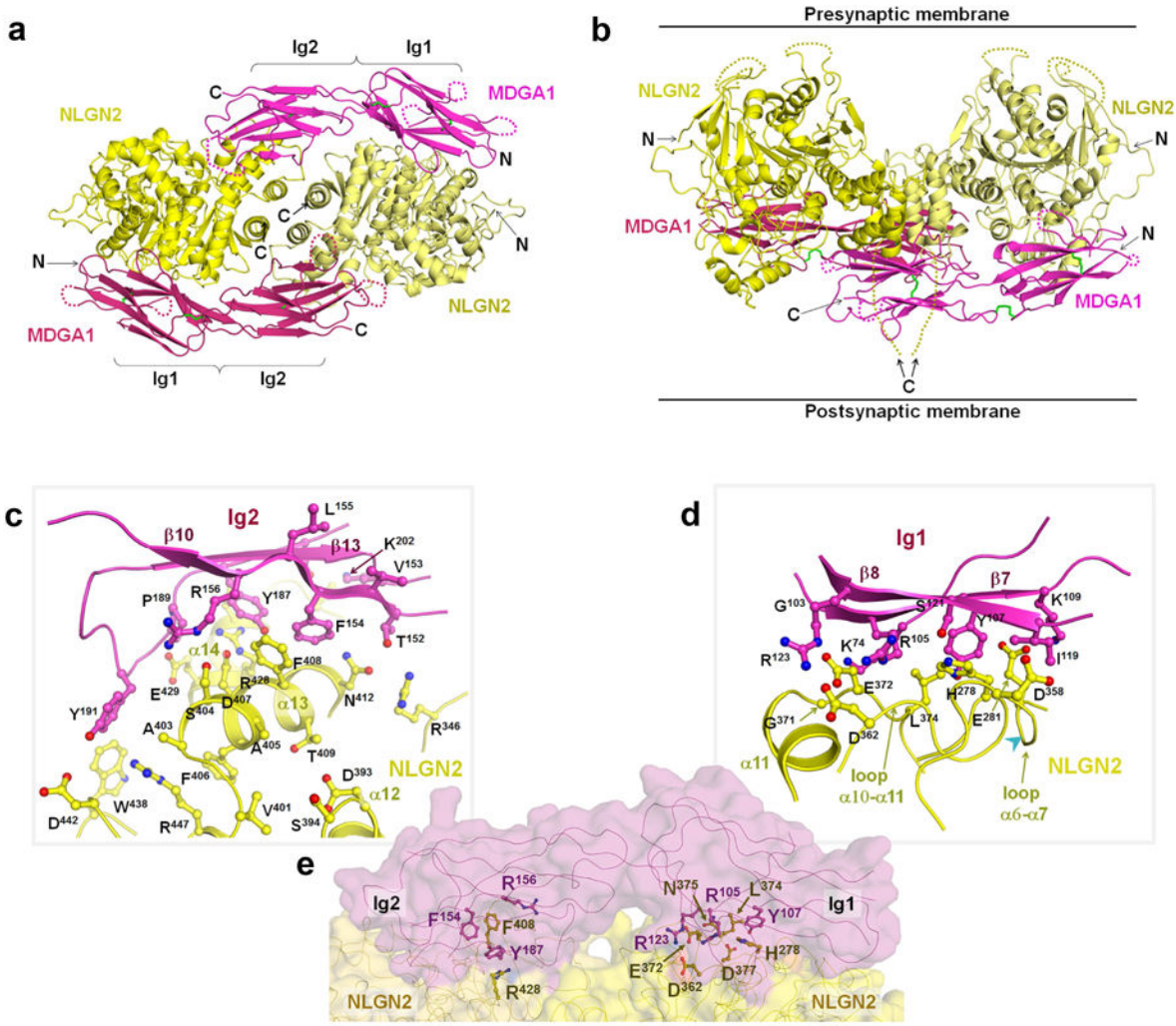

f

Mutant	mutated residues	TMR-MDGA1-C8 K_D (nM)	TMR-n1α L5L6 K_D (nM)
NL2-Mut1	$H^{278}A$, $D^{362}K$, $E^{372}K$	—	43.5 ± 33.2
NL2-Mut3	$H^{278}A$, $D^{362}K$, $E^{372}K$, $F^{408}A$, $R^{428}A$	—	35.2 ± 24.1
NL2-Mut4	$H^{278}A$, $D^{362}A$, $E^{372}A$	76.9 ± 48.7	25.1 ± 12.0
NL2-Mut5	$H^{278}A$, $D^{362}A$, $E^{372}A$, $F^{408}A$, $R^{428}A$	138.0 ± 82.1	14.5 ± 7.4
NL2-Mut6	$L^{374}A$, $N^{375}A$, $D^{377}A$	70.0 ± 34.6	27.6 ± 21.6
NL2-wt	none	7.8 ± 4.9	17.6 ± 7.1

g

Mutant	mutated residues	NLGN2 K_D (nM)
hMDGA1 C8_Mut1	$R^{105}E$, $Y^{107}A$, $R^{123}E$, $F^{154}A$, $R^{156}A$, $Y^{187}A$	91.1 ± 23.7
hMDGA1 C8_Mut2	$R^{105}E$, $Y^{107}A$, $R^{123}E$	189.9 ± 52.0
hMDGA1 C8_Mut3	$F^{154}A$, $R^{156}A$, $Y^{187}A$	105.1 ± 39.0
hMDGA1 C8_Mut4	$R^{105}A$, $Y^{107}A$, $R^{123}A$, $F^{154}A$, $R^{156}A$, $Y^{187}A$	379.6 ± 232.5
hMDGA1 C8_Mut5	$R^{105}A$, $Y^{107}A$, $R^{123}A$	249.3 ± 170.2
hMDGA1 C8_wt	none	48.4 ± 28.0

Figure 3. MDGA1 Ig1–Ig2:NLGN2 complex

(A) Ribbon diagram of the complex as viewed from the post-synaptic membrane. **(B)** Ribbon diagram of the complex viewed sideways as it fits in the synaptic cleft. Disulfide bonds are shown in green. (**C** and **D**) Interface between MDGA1 Ig2 (left) and Ig1 (right) with NLGN2. A cyan arrow pointing to loop α6–α7 in **(D)** indicates where NLGN1 site B would insert. **(E)** Residues targeted for site-directed mutagenesis in MDGA1 (magenta), and in NLGN2 (yellow). **(F)** Binding of NLGN2 mutants to TMR-MDGA1 Ig1–Ig2 and TMR-n1α L5L6 in an FP-based assay. '—' indicates no significant binding. **(G)** Binding of TMR-MDGA1 Ig1–Ig2 mutants to NLGN2 in a FP-based assay. In **(F)** and **(G)** the K_D values

were averaged over two independent experiments carried out on separate days (mean ± standard deviation).

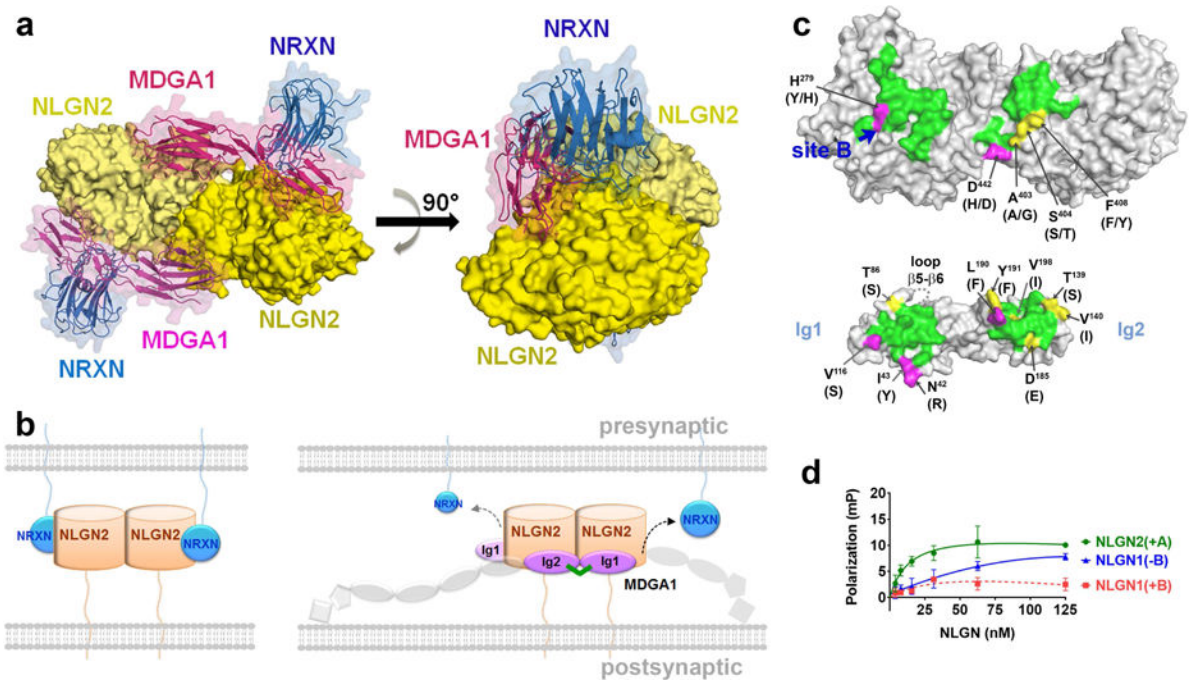

Figure 4. Mechanism of NLGN2 regulation by MDGA1

(A) NLGN2:MDGA1 Ig1–Ig2 complex superimposed with the NLGN1:neurexin 1β complex (PDB ID: 3B3Q; neurexin in blue, NLGN1 not shown for the sake of clarity). Note: the amino acid sequence of the LNS domains in neurexin 1β and neurexin 1α L6 are identical. **(B)** The neurexin-neuroligin trans-synaptic bridge promotes synapse development and stabilization at inhibitory synapses (left). MDGA1 binds to NLGN2 obstructing the latter's binding site for neurexin sterically, by interacting with a partially overlapping binding site; this hinders the formation of the NLGN2:neurexin trans-synaptic bridge (right). **(C)** *Top:* sequence conservation of the MDGA1 interaction site mapped onto the surface of the NLGN2 dimer between NLGN1, NLGN2, NLGN3 (human, bovine, rat, mouse). Equivalent residues in NLGN1/NLGN3 are shown in parentheses. The NLGN1 site B insert is indicated with a blue arrow; the colored patch on the left corresponds with the Ig1 binding site; the colored patch on the right with the Ig2 binding site. *Bottom:* sequence conservation of the NLGN2 interaction site mapped onto the surface of MDGA1 between MDGA1 and MDGA2 (human, bovine, rat, mouse). Equivalent residues in MDGA2 are shown in parentheses. Conserved (green), semi-conserved (yellow) and non-conserved (magenta). **(D)** Binding of TMR-MDGA1 Ig1–Ig2 to NLGN2, NLGN1(+B) or NLGN1 (no insert) monitored in a FP-binding assay.

Table 1

	MDGA1 Ig1–Ig2	NLGN2-MDGA1 Ig1–Ig2
Data collection		
Wavelength (Å)	0.97918 Å	0.97872 Å
Space group	I23	P1
Cell dimensions		
a, *b*, *c* (Å)	139.07, 139.07,139.07	103.12, 97.18, 190.51
α, β, γ (°)	90, 90, 90	95.52, 80.97, 88.71
Resolution (Å)*	32.78–2.71 (2.76–2.71)	49.77–4.11 (4.18–4.11)
Total/Unique reflections *	69,618/12,205 (617)	201,426/53,553 (2112)
R_{merge} (%) *	0.064 (0.945)	0.064 (0.586)
$I/\sigma I$*	26.0 (2.0)	18.8 (2.0)
Completeness (%) *	99.7 (100.0)	94.4 (76.1)
Multiplicity *	5.8 (5.7)	3.8 (3.5)
Refinement&		
Resolution (Å)	32.8–2.7	49.8–4.1
R_{work}/R_{free} (%)	0.212/0.260	0.272/0.296
Model (no. atoms)	1590	33540
Protein (no. residues)	198	4266
Ligands	3 $SO4^{2-}$, Cl^{-}	0
Waters	10	0
B factors		
Protein (Å^2)	57.6	n.r.
Ligands (Å^2)	81.6	n.r.
Waters (Å^2)	29.2	n.r.
r.m.s. deviations		
Bond lengths (Å)	0.004	0.030
Bond angles (°)	0.704	1.838
Ramachandran plot residues (%)		
Favored	182 (95.8%)	3476 (84.1%)
Allowed	8 (4.2%)	570 (13.8%)
Disallowed	0 (0.0%)	88 (2.1%)
Molprobity Overall Score	1.1	2.7

* numbers in parentheses refer to the highest resolution data shell;

& statistics as provided by Phenix (Molprobity);

r.m.s., root-mean-square;

n.r., individual B-factors not refined